

# Design and Performance Research on Dual Layer Cement Based Absorber Reinforced with Graphene Nanosheets and Manganese-zinc Ferrite

Yafei SUN<sup>1,2,\*</sup>, Tianshu ZHOU<sup>3</sup>, Yueyue PENG<sup>4</sup>, Hongwei LIU<sup>1</sup>

<sup>1</sup> Department of Civil Engineering, Yancheng Institute of Technology, 1 Hope Avenue, Yancheng, 224051, China

<sup>2</sup> Department of Civil Engineering, Nanjing University of Aeronautics and Astronautics, 29 General Avenue, Nanjing 210016, China

<sup>3</sup> Department of Civil Engineering Mechanics, Jiangsu University, 301 Xuefu Road, Zhenjiang 212013, China

<sup>4</sup> Department of Civil Engineering, Anhui University of Science and Technology, 168 Taifeng Avenue, Huainan 232000, China

**crossref** <http://dx.doi.org/10.5755/j02.ms.24680>

Received 25 November 2019; accepted 24 March 2020

Dual layer cement-based absorber is synthesized by mixing with graphene nanosheets and manganese-zinc ferrite, to study the effect of absorbing filler content on the mechanical properties, microstructure, electrical resistivity and reflectivity of the paste. The microstructure of the absorber is seen by Scanning Electron Microscope (SEM) images, Fourier Transform Infrared (FTIR) spectroscopy, X-Ray Diffraction (XRD) curves of the absorber. The results show that graphene nanosheets significantly reduce the electrical resistivity of paste, increasing its mechanical properties by improving its pore structure. SEM images indicate that graphene nanosheets promote the increase and coarsening of cement hydration products and produce a large number of dense bulk crystals. Furthermore, reflectivity measurements show that the minimum reflectivity of  $-14.1$  dB is obtained in the range of  $2 \sim 18$  GHz and the effective bandwidth of  $16$  GHz is obtained when reflectivity is less than  $-7$  dB. This study provides a new method for the preparation of dual layer cement-based absorber.

**Keywords:** graphene nanosheets, microstructure, electrical resistivity, mechanical properties, reflectivity.

## 1. INTRODUCTION

Traditional cement-based composite materials have been widely used in infrastructure projects such as buildings, roads, bridges, tunnels, and ports due to their excellent environmental adaptability, low price, and easy access to materials. With the rapid development of the construction industry, high-performance cement-based materials (high-performance concrete and mortar) have become an urgent need, and mixing fillers in cement-based materials is an important way to improve their rheological properties, strength, durability, electrical conductivity and absorbing properties [1, 2]. Therefore, nanomaterials with surface size effect, quantum Hall effect, macroscopic quantum tunneling effect and dielectric confinement effect have become a new type of microwave absorber with potential application value.

In recent years, many scholars have carried out substantial researches on the application of graphene nanosheets (NGPs) and reduced graphene oxide (rGO) in cement-based materials and achieved fruitful results. Silva et al. [3] reported that the 3d, 7d and 28d compressive strength of mortar with 0.021% NGPs increases by 63.6 %, 94.1 % and 95.7 % respectively compared with that of ordinary mortar. Sun et al. [4] studied the electrical response of mortar with NGPs under different loading amplitudes and loading rates. Meanwhile, the application of mortar with NGPs in dynamic loading rate measurement was discussed, the results show that the mortar with NGPs is sensitive to pressure and its resistivity varies steadily with pressure under different loading conditions. Huang [5] found that the flexural strength and electric of cement-based composites is

significantly improved by adding NGPs, and its flexural strength is increased by 82% compared with that of control specimens.

Besides, rGO possesses excellent intrinsic properties of NGPs [6–10]. There are a large number of active groups in its structure, which make it hydrophilic and easy to be dispersed to prepare nano-dispersions. A small load of rGO can accelerate the hydration process of cement, promote the formation of hydration products as well as improve the pore structure and mechanical properties of cement-based materials. rGO-CF composites were prepared by Chen et al. [11] using electrophoretic deposition, which prepared reduced graphene oxide (rGO) on the surface of carbon fibers (CF). The results show that the absorbing property in X-band ( $8.2 \sim 12.4$  GHz) of the cement-based materials with 0.4 wt.% of rGO-CF is 31 % higher than that of the cement-based materials with 0.4 wt.% of CF.

Manganese-zinc ferrite (MZF) is made of iron, manganese, zinc oxides and other salts by ceramic process. It has spinel structure, high saturation magnetization, and initial permeability as well as low coercivity. Its natural resonance is the main mechanism of absorbing electromagnetic waves. At the same time, it has large electric hysteresis loss as ferroelectric materials and large magnetic hysteresis loss as ferromagnetic materials, so MZF can obtain large electromagnetic wave absorption capacity. As mentioned above, it has been reported that NGPs can improve the pore structure, hydration process and mechanical properties of paste. However, there are few researches on the preparation of two-layer cement-based

\* Corresponding author: Tel.: (086)15005113689; fax: (086)051588168205. E mail address: 2987939688@qq.com (Y. Sun)

microwave absorbers by stratified mixing NGPs, MZF, MWCNTs and Carbon black (CB) into paste. In this paper, the effects of NGPs, MZF, MWCNTs and CB on the microstructure, resistivity, mechanical strength and microwave absorbing properties of paste are investigated, and the theoretical discussion is made for the development of a new type of dual layer cement based absorber (Board made of wave absorbent).

## 2. STRUCTURAL DESIGN

According to electromagnetic wave shielding and absorption theory, the ideal absorber should have the following conditions: 1) It can make the incident electromagnetic wave enter the material to the maximum extent and has the characteristics of wave impedance matching; 2) It can attenuate the incident electromagnetic wave as far as possible, convert it into heat energy or other forms of energy and have the attenuation characteristics; 3) The same type of material can effectively absorb multi-band electromagnetic wave and has broadband characteristics; 4) It is hard to react with other components in various environments as well as have high stability characteristics; 5) It possesses good wear resistance and weatherability as well as good mechanical properties; 6) It has the advantages of thin thickness, light weight, easy construction, low cost and practical engineering characteristics. It is difficult to achieve the goal of impedance matching and broadband absorption for single-layer structure materials doped with a single type of absorbent, and composite is an effective way to solve such problems. The design of absorber fundamentally solves problems such as impedance matching and plate thickness, absorbing efficiency and absorbing bandwidth, shape and structure.

Portland cement-based materials is a kind of electromagnetic wave-transmitting materials with high dielectric constant. Zhang et al. [12] showed that the real part ( $\epsilon'$ ) of permittivity ( $\epsilon$ ) in paste is about 6.75–7.0 and its imaginary part is 6.75–7.0. Therefore, the absorption performance of absorber mainly depends on the type and content of absorbing filler.

The upper layer mixing with magnetic absorbent is designed to absorb mostly the electromagnetic wave, which will make electromagnetism energy transform into heat energy, so as it dissipates or disappears. The lower layer mixed with resistive or dielectric absorbent is designed as reflection layer, where a conductive network is formed by utilizing carbon-based materials with high conductivity. So that part of the electromagnetic wave will be consumed by the multiple reflection and make electromagnetism energy

**Table 1.** Mix proportion

No.	NGPs, %	MZF, %	MWCNTs, %	CB, %	Silica fume, %	Water reducer, %	W/C, %	Thickness of board, mm	Amount of cement, g
F0					10	0.32	0.31	30	3482
GPF1	Up	0.03	15			10	0.33	0.32	16
	Down			0.5	4	10	0.35	0.44	14
GPF2	Up	0.05	15			10	0.33	0.33	16
	Down			0.5	4	10	0.35	0.44	14
GPF3	Up	0.03	25			10	0.34	0.33	16
	Down			0.5	4	10	0.35	0.44	14

transform into heat energy, so as it dissipates or disappears.

In this paper, dual layer cement-based absorber is synthesized by mixing with the resistance type, dielectric type and magnetic type microwave absorbents based on this structural design idea as well as combined with the previous research results of our group. The mix ratio and thickness of the absorber in this paper as shown in Table 1 was designed to ensure the similar fluidity of paste (taking cement quality as one unit), and the specimen size is  $300 \times 300 \times 30 \text{ mm}^3$ .

## 3. EXPERIMENTAL PROCEDURE

### 3.1. Material

The cementitious materials are P. II 42.5 Portland Cement that the quality meets the requirements of General Portland Cement (GB175–2007), produced by Jiangsu Conch Cement Plant and silica fume was supplied from Shanghai Litian Silicon Powder Material Co., Ltd. Experiments were conducted with NGPs and MWCNTs (Zhongke Leiming Technology Co., Ltd.). Polyhedron like MZF (Hebei Shijiazhuang Yulei Building Material Co., Ltd.) has an iron content over than 90 % and its particle size is 180 ~ 1250 meshes. Whereas, polycarboxylic acid super plasticizer (Shanghai Sanrui Polymer Materials Technology Co., Ltd.) with a water reduction rate of 45 % is used to enhance the fluidity of paste. White flocculent powder carboxymethyl cellulose is used as dispersant (Hebei Xingtai Cellulose Co., Ltd.). The properties of NGPs, MWCNTs and silica fume are shown in Tables 2, Table 3 and Table 4.

**Table 2.** Performance index of NGPs

Purity	Thickness	Diameter
> 99.5 wt. %	0.4 ~ 20 nm	5 ~ 10 $\mu\text{m}$
Layers	Density	Volumetric resistivity
1 ~ 5 layers	0.23 g/cm <sup>3</sup>	$4 \times 10^{-4} \text{ ohm}\cdot\text{cm}$

**Table 3.** Performance indexes of MWCNTs

Purity	Diameter	Length
> 98 wt. %	20 ~ 30 nm	10 ~ 30 $\mu\text{m}$
Specific area	Stacking density	Conductivity
> 110 m <sup>2</sup> /g	0.27 g/cm <sup>3</sup>	150 s/cm

**Table 3.** Performance indexes of MWCNTs

Purity	Diameter	Length
> 98 wt. %	20 ~ 30 nm	10 ~ 30 $\mu\text{m}$
Specific area	Stacking density	Conductivity
> 110 m <sup>2</sup> /g	0.27 g/cm <sup>3</sup>	150 s/cm

**Table 4.** Performance index of silica fume

Total alkalinity	Content of SiO <sub>2</sub>	Specific surface area
< 1.5 %	> 85 %	66 m <sup>2</sup> /g
Activity index	Water content	Water demand ratio
> 105 %	< 3.0 %	< 125 %

The main apparatuses used in the test are NJ-160A grouting machine is manufactured by Wuxi Jianyi Instrument Machinery Co., Ltd., BS-110S electronic analytical balance manufactured by Beijing Sedoris Balance Company, field emission scanning electron microscope (Nova Nano SEM 450) is manufactured by Thermo Electron Corporation of the United States, MF47F multimeter is manufactured by Nanjing Tianyu Electronic Instrument Factory and HP8722ES vector network analyzer is manufactured by Shenzhen Xintong Electronic Instrument Co., Ltd., DHG-9146A electro-thermal thermostatic blasted drying oven is manufactured by Shanghai Jinghong Experimental Equipment Co., Ltd., microcomputer controlled electronic universal testing machine is manufactured by Wuxi Zhongke Building Materials Co., Ltd., MF47F multimeter is manufactured by Nanjing Tianyu Electronic Instrument Factory and HP8722ES vector network analyzer is manufactured by Shenzhen Xintong Electronic Instrument Co., Ltd.

### 3.2. Test method

1) Paste preparation: Silica fume, cement and MZF were first added into a planetary mixer and stirred evenly, then add NGPs dispersion, water and water reducer, stirred at low speed for 2.5 min, stopped for the 20 s, then stirred for 2.5 min at high speed, the paste for the upper layer was prepared. Cement, silica fume and MZF into a planetary mixer and stirred evenly, then add water and water reducer, stirred at low speed for 2.5 min, stopped for the 20 s, then stirred for 2.5 min at high speed, the paste for the lower layer was prepared.

2) Specimen preparation: The double-layer stacking molds were used according to the design dimensions of dual-layer structure. The resultant mixture was poured into in 40 × 40 × 160 mm<sup>3</sup> and 25 × 25 × 25 mm<sup>3</sup> oiled stacking molds respectively. Mechanical and electrical conductivity tests were carried out, and the specimens were shaped by vibration. After that, two 16 mm × 30 mm copper wire electrodes were embedded in the specimen and the resistivity was measured at about 5 mm away from both ends of the specimen. The size of the reflectivity test specimen is 180 × 180 × 30 mm<sup>3</sup>. At least three samples were made in each group and placed in standard curing box (Temperature is 20 ± 2 °C, relative humidity is more than 90 %) for 28d subsequently.

3) Test method: According to DL/T 5126-2001, the strength of the samples was tested by the universal testing machine. The compressive strength of specimens was tested under the load-controlled mode with a loading rate of 2.4 kN/s using the WDW-E2000 microcomputer controlled electronic universal testing machine. The flexural strength of samples was tested at 20 N/s loading rate. Whereas, the compressive strength of samples can be calculated as follows:

$$R_c = F_c / A; \quad (1)$$

where  $F_c$  is the failure load of sample,  $A$ : is the cross-section area of the sample.

The flexural strength of samples can be calculated as follows:

$$R_f = 1.5F_f L / b^3; \quad (2)$$

where  $F_f$  is the failure load of the sample,  $L$  is the distance between the two support cylinders,  $b$  is the length of the cross-section of the sample.

The electrical resistance  $R$  ( $\Omega$ ) of the specimens for 3d, 7d and 28d is measured by the multimeter, the distance between the two electrodes is  $L$  (cm), the cross-section area of the specimen is  $A$  (cm<sup>2</sup>), and the electrical resistivity of specimens can be calculated by  $\rho = RA/L$ .

The reflectivity measurement system is a bow system composed of vector network analyzer, test antenna and signal source. This test is carried out according to the "Radar Absorbing Material Test Standard" (GJB2038-2011).

## 4. RESULTS AND DISCUSSION

### 4.1. The characterization of NGPs

Fig. 1 shows the TEM images of NGPs.

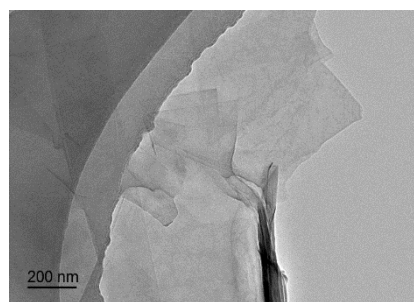


**Fig. 1.** TEM images of NGPs

TEM images shows the unique two-dimensional corrugated structure of NGPs with a high aspect ratio. The shape of NGPs is like a transparent film with rough surface, which makes it possible for NGPs to adsorb heterogeneous particles for modification. Meanwhile, the corrugated structure also increases the contact area between the matrix of cement-based material, resulting in higher bonding force and pull-out force, thus enhancing the mechanical properties of the composite. As shown in Fig. 1, the diameter of NGPs is about 5 ~ 10  $\mu$ m, and its thickness is about 0.5 ~ 20 nm.

### 4.2. Infrared analysis

Fig. 2 displays the infrared spectrum of the specimen F0 and specimen GPF1 ~ GPF3. As can be seen in Fig. 2, near 3442 cm<sup>-1</sup> has a broad absorption band, which corresponds to the antisymmetric flexural vibration band of O-H. And the sharp peak at 3801 cm<sup>-1</sup> are attribute to the stretching vibration of free O-H bond. The peak at 1631 cm<sup>-1</sup> is attributed to the skeleton vibration of C=C and C-C bonds in NGPs, the peak near 1425 cm<sup>-1</sup> is attributed to the flexural vibration of O=C-O, and the peak near 1121 cm<sup>-1</sup> corresponds to the stretching vibration of C=C as well as the peak near 876 cm<sup>-1</sup> are the flexural vibration of C-H on the phenyl ring structure of graphene indicating that NGPs has

been added in specimens.

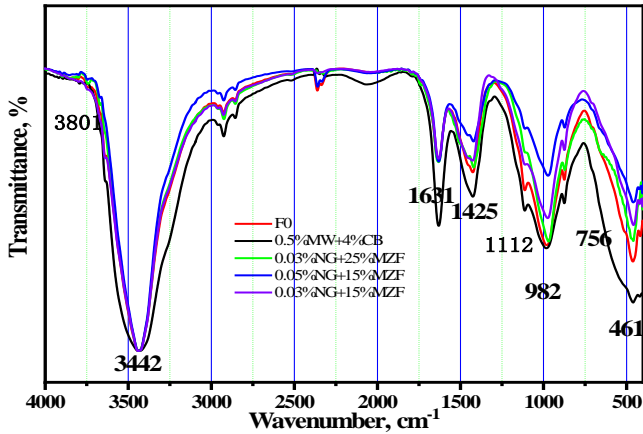


Fig. 2. IR spectra of specimens

In addition, the peak at  $461\text{ cm}^{-1}$  is attributed to the stretching vibration peak [13] of Fe-O bond, which indicates that MZF is mixed into paste.

### 4.3. The analysis of mechanical properties

Fig. 3 shows that the compressive strengths of the upper layer in paste with NGPs and MZF at 7 days and 28 days increase obviously with the increase of NGPs content. The compressive strength of the upper layer of specimen GPF2 at 7 days and 28 days are 77.8 MPa and 103.5 MPa, respectively, which are increased by 14.7 % and 15.4 % compared with that of specimen GPF1 and increased by 30.3 % and 32.7 % compared with that of specimen F0. This result conforms to the results of Mohamed Saafi et al [14]. The improvement of mechanical properties of upper layer is attributed to the addition of NGPs. Because NGPs with unique corrugated structures can be used as templates to provide sites hydrated crystals in the hydration process, the hydrated product crystals are hardened and play an important role in reinforcing and toughening the paste.

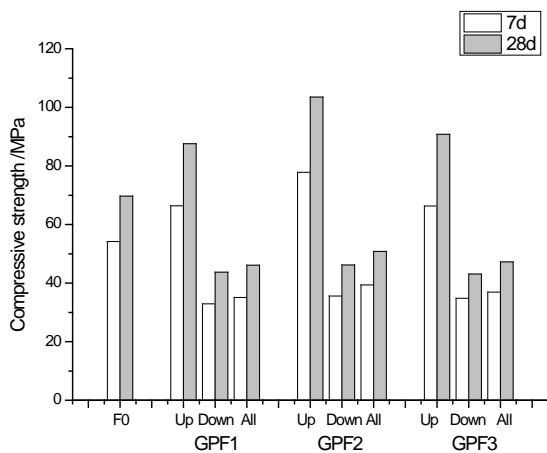


Fig. 3. Compressive strength of paste

The compressive strength of the down layer of specimen GPF1 at 7 days and 28 days are 32.9 MPa and 43.7 MPa, respectively, which are reduced by 39.3 % and 37.3 % compared with that of specimen F0. Because the "ball effect" caused by the incorporation of CB in the matrix reduces the interfacial effect in the matrix. It can also be seen from Fig. 3 that the value of compressive strength of

dual-layer specimen GPF1 ~ GPF3 is between that of the upper layer and the down layer, and is close to that of the down layer. According to the non-linear theory of composite materials, the overall strength of composite is usually determined by the lower strength part of composite.

### 4.4. The conductivity of paste

Fig. 4 shows the resistivity of paste can be effectively reduced when added with absorbing filler, especially at 3 days and 7 days compared with specimen F0, and the value of resistance can vary in the order of  $10^2 \sim 10^3 \Omega \cdot \text{cm}$ . The resistivity of the specimen with 0.5 % MWCNTs + 4 % CB in the lower layer is in consistent with the results of Chen et al. [15].

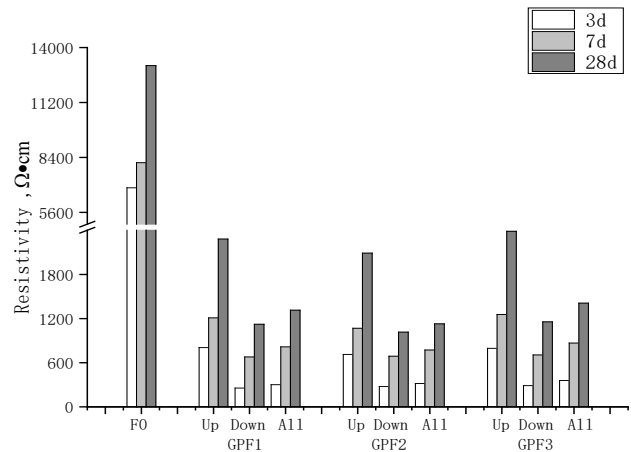


Fig. 4. Resistivity of paste

The resistivity of the upper layer is quite higher because of the amount and type of absorbent. Due to the small content of nanoparticles in the matrix, the dispersion is irregular, and the distance between the nanoparticles is too large to cross the barrier, the effect on the electrical conductivity of composites is shown. In this experiment, the content of NGPs with favorable conductivity is too low to form a closed or connected conducting network, therefore, it has little influence on the resistivity of composite. The effect of the content of MZF on the resistivity in absorber is small although the content of MZF is large due to its high resistivity. Both MWCNTs and CB in the lower layer have excellent electrical conductivity, which is conducive to form conductive network and make the resistivity of composites significantly lower. The 28d resistivity is obviously higher than that of 7d for one specimen. With the growth of age, the free water molecules in the matrix reduces continuously, and the possibility of water molecules connecting with nano-absorbents decreases, which leads to the increase of resistivity. It can also be seen from Fig. 3 that the value of compressive strength of dual-layer specimen GPF1-3 is between that of the upper layer and the down layer, and is close to that of the down layer. Meanwhile, it can be seen that the value of overall resistivity of specimen is between that of the upper layer and the down layer, and is close to that of the down layer. And it is about 1.1 ~ 1.25 times of the resistivity of the lower absorbing layer. Double-layer absorber can be abstractly regarded as two resistors with different values connected in parallel. According to Ohm's law, parallel resistance is closer to the resistance with

smaller values.

According to Schelkunoff's formula, the electromagnetic wave absorption performance of materials is related to their conductivity and permeability, and it increases with the increase of conductivity and permeability. Consequently, resistivity is one of the main factors affecting the absorption performance of materials. Pierre R et al. found that materials with resistivity values ranging from  $10 \Omega \cdot \text{cm}$  to  $103 \Omega \cdot \text{cm}$ , have good electromagnetic shielding and absorption ability [16].

#### 4.5. SEM analysis

Fig. 5 shows SEM images of specimen GNF1 ~ GNF3 with different amount of microwave absorbent to study the effect of NGPs content and other absorbing filler contents on the hydration and crystallization products of paste. SEM images show that AFt, AFm, CH and C-S-H gels, as well as a large number of flake and dense block crystals, are the main crystallization products of paste with nano-absorbents. With the change of nano-absorbent content, the crystals show different shapes Fig. 5 a shows that layered crystals with dense texture are neatly stacked together; Large crystals with smooth surface and dense texture can be observed in Fig. 5 b;

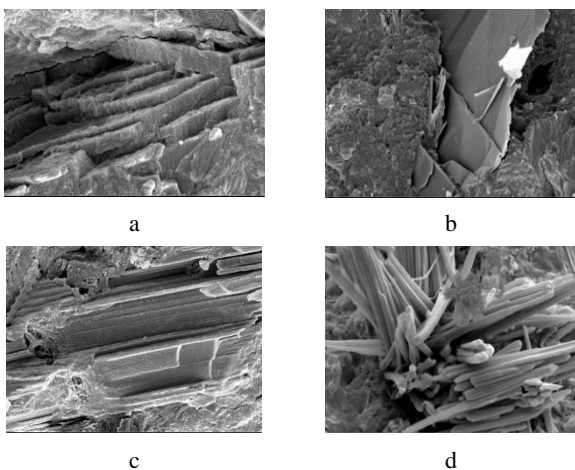


**Fig. 5.** SEM images of samples at 28 days:  
a - 0.03 % NGPs + 15 % MZF;  
b - 0.03 % NGPs + 25 % MZF;  
c - 0.05 % NGPs + 15 % MZF;  
d - 0.5 % MWCNTs + 4 % CB

Large columnar crystals with dense and clear texture can be observed in Fig. 5 c; A large number of rod crystals with dense crystal structure and fluffy texture can be observed uniformly clustered in Fig. 5 d, which is also the reason for the significant decrease in mechanical properties. Zhao et al. [17] found that NGPs with large specific surface area, can absorb plenty of free water and provide free water for the adjacent unhydrated particles with the development of the hydration reaction, thus forming larger block or column hydrated crystals on the surface of NGPs, which can significantly improve the mechanical properties of paste.

#### 4.6. The reflectivity of paste

According to the electromagnetic shielding theory, reflectivity is an important indicator for evaluating the absorbing properties. Therefore, when the reflectivity of

absorbing material is less than  $-5\text{dB}$ , the electromagnetic wave absorbing and shielding materials can be used in general buildings, and when the reflectivity of absorbing material is less than  $-7\text{dB}$  [18], the electromagnetic wave absorbing and shielding materials can be reliably used in critical military equipment or facilities. [18]. The test results of 28d reflectivity for GPF1 ~ GPF3 are shown in Fig. 6.

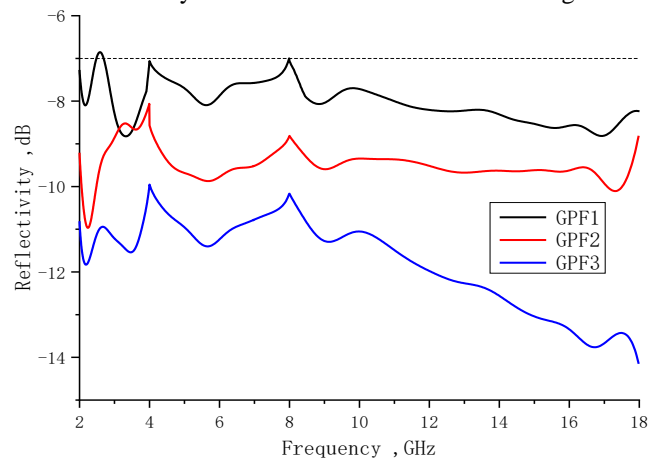


**Fig. 6.** Reflectivity of cement-based absorber

Fig. 6 shows the minimum reflectivity of GPF1 as appeared at 3.33 GHz, reaching to  $-8.8 \text{ dB}$ . When it is less than  $-7\text{dB}$ , effective bandwidth can be achieved to 15.8 GHz. When the minimum reflectivity of GPF2 appeared at 2.19 GHz, reaching to  $-11.8\text{dB}$ , it is less than  $-7 \text{ dB}$ , effective bandwidth can be achieved to 16 GHz.

It can be seen that the reflectivity is significantly affected by the GNPs content. Because the absorbing reflectivity of specimen GPF2 is lower than that of specimen GPF1, when the frequency is in the range of 2 ~ 18 GHz. Besides, the absorbing reflectivity of specimen GPF3 is lower than that of specimen GPF2, and it shows that the effect of MZF content on reflectivity is more obvious than that of GNPs, which may be by the small content of GNPs. Fig. 6 shows that the minimum reflectivity of the absorber is less than  $-7 \text{ dB}$  in the range of 2 ~ 18 GHz, which proves that the absorbers achieve full coverage test frequency and the target of broadband absorption. Thereafter, a proper amount of nanofiller is fully mixed to form a closed conductive network, and part of the electromagnetic wave is converted into thermal energy by inner generated vortex part. At the same time, MZF, as magnetic absorbing filler, has greater effective anisotropy, which leads to higher hysteresis loss of cement-based absorbers. These mechanisms enable the cement-based absorbers to absorb electromagnetic waves very well.

## 5. CONCLUSIONS

1. The compressive strength of paste with 0.05 % NGPs at 7 days and 28 days are increased by 30.3 % and 32.7% compared with that of specimen F0. It indicates that low content of NGPs can significantly improve the compressive strength of paste, which is attributed to the unique corrugated structure and large specific surface area of NGPs, which increases the contact area between the substrate and NGPs, produces higher adhesion and tensile strength, and enhances the mechanical strength of the composite.

2. NGPs and MZF possess excellent absorbing properties, and their content has a significant effect on the absorbing properties of paste. The reflectivity test results show that the influences of the MZF on the absorbing properties of paste were more obviously than NGPs.
3. The two-layer structure absorber has better absorption performance than the single-layer structure absorber studied earlier by our project group, especially in the frequency range of 8 ~ 18 GHz. Its reflectivity decreases significantly with the increase of frequency and achieve the full coverage test frequency as well as the target of broadband absorption. The research results change the decreasing trend of mechanical properties of cement-based microwave absorbing materials when mixed with traditional absorbents. In important civil buildings and military installations, the electromagnetic shielding and absorption of double-layer absorbing materials prepared has potential application prospects.

### Acknowledgements

The authors would like to acknowledge the Joint Research Fund of Jiangsu Province (BY2016065-27) and the Chinese National Natural Science Fund Project (51478408) for its financial support in this project.

### REFERENCE

1. Gencil, O., Ozel, C., Brostow, W., Martínez-Barrera, G. Mechanical Properties of Self-compacting Concrete Reinforced with Polypropylene Fibres *Materials Research Innovations* 15 (3) 2011: pp. 216–225. <https://doi.org/10.1179/143307511X13018917925900>
2. Martínez-Barrera, G., Viguera, E., Gencil, O., Hagg Lobland, H.E. Polymer Concretes: A Description and Methods for Modification and Improvement *Journal of Materials Education* 33 (1–2) 2011: pp. 37–52.
3. Silva, R.A.E., Paulo, D.C.G., Luz, M.S.D., Rouxinol, F., Gelamo, R.V. Enhanced Properties of Cement Mortars with Multilayer Graphene Nanoparticles *Construction and Building Materials* 149 2017: pp. 378–385. <https://doi.org/10.1016/j.conbuildmat.2017.05.146>
4. Sun, S.W., Han, B.G., Jiang, S., Yu, X., Wang, Y., Li, H.Y., Ou, J.P. Nano Graphene Platelets-enabled Piezoresistive Cementitious Composites for Structural Health Monitoring *Construction and Building Materials* 136 2017: pp. 314–328. <https://doi.org/10.1016/j.conbuildmat.2017.01.006>
5. Huang, S. Multifunctional Graphite Nanoplatelets (GNP) Reinforced Cementitious Composites, Masters thesis, 2012.
6. Sun, Y.F., Chen, M., Gao, P.W., Zhou, T.S., Liu, H.W., Xun, Y. Microstructure and Microwave Absorbing Properties of Reduced Graphene Oxide/Ni/multi-walled Carbon Nanotubes/Fe<sub>3</sub>O<sub>4</sub> Filled Monolayer Cement-based Absorber *Advances in Mechanical Engineering* 11 (1) 2019: pp. 1–11. <https://doi.org/10.1177/1687814018822886>
7. Ahmadzadeh, N., Rashidan, Z., Baharvand, A. Gate-controlled Conductance in ABA-Stacked Trilayer Graphene *Iranian Journal of Science and Technology* 43 2019: pp. 2657–2663. <http://doi.org/10.1007/s40995-019-00716-2>
8. Rajaura, R.S., Sharma, V., Ronin, R.S., Gupta, D.K., Srivastava, S., Agrawal, K., Vijay, Y.K. Synthesis, Characterization and Enhanced Antimicrobial Activity of Reduced Graphene Oxide–zinc Oxide Nanocomposite *Materials Research Express* 4 (2) 2017: pp. 025401. <http://doi.org/10.1088/2053-1591/aa5bffTI>
9. Yang, H., Monasterio, M., Cui, H., Han, N. Experimental Study of the Effects of Graphene Oxide on Microstructure and Properties of Cement Paste Composite *Composites Part A* 102 2017: pp. 263–272. <https://doi.org/10.1016/j.compositesa.2017.07.022>
10. Paz, E., Forriol, F., del Real, J.C., Dunne, N. Graphene Oxide Versus Graphene for Optimisation of PMMA Bone Cement for Orthopaedic Applications *Materials Science & Engineering C* 77 2017: pp. 1003–1011. <https://doi.org/10.1016/j.msec.2017.03.269>
11. Chen, J., Zhao, D., Ge, H., Wang, J. Graphene Oxide-deposited Carbon Fiber/Cement Composites for Electromagnetic Interference Shielding Application *Construction and Building Materials* 84 2015: pp. 66–72. <https://doi.org/10.1016/j.conbuildmat.2015.03.050>
12. Zhang, X., Sun, W. Preparation and Microwave Absorbing Properties of Three-layered Cement-based Composites *Procedia Engineering* 27 2012: pp. 348–356. <https://doi.org/10.1016/j.proeng.2011.12.462>
13. Deng, J., Feng, S.F., Ma, X., Tan, C., Wang, H., Zhou, T.S., Li, Z.J. Heterogeneous Degradation of Orange II with Peroxymonosulfate Activated by Ordered Mesoporous MnFe<sub>2</sub>O<sub>4</sub> *Separation and Purification Technology* 167 2016: pp. 181–189. <https://doi.org/10.1016/j.seppur.2016.04.035>
14. Saafi, M., Tang, L., Fung, J., Rahman, M., Liggat, J. Enhanced Properties of Graphene/Fly Ash Geopolymeric Gcomposite Cement *Cement and Concrete Research* 67 2015: pp. 292–299. <https://doi.org/10.1016/j.cemconres.2014.08.011>
15. Chen, M., Gao, P., Geng, F., Zhang, L., Liu, H. Mechanical and Smart Properties of Carbon Fiber and Graphite Conductive Concrete for Internal Damage Monitoring of Structure *Construction and Building Materials* 142 2017: pp. 320–327. <https://doi.org/10.1016/j.conbuildmat.2017.03.048>
16. Richard, P., Cheyrezy, M. Composition of Reactive Powder Concretes *Cement and Concrete Research* 25 (7) 1995: pp. 1501–1511. [https://doi.org/10.1016/0008-8846\(95\)00144-2](https://doi.org/10.1016/0008-8846(95)00144-2)
17. Zhao, L., Guo, X., Ge, C., Li, Q., Guo, L. Investigation of the Effectiveness of PC@GO on the Reinforcement for Cement Composites *Construction and Building Materials* 113 2016: pp. 470–478. <https://doi.org/10.1016/j.conbuildmat.2016.03.090>
18. Sun, Y.F., Gao, P.W., Peng, H.L., Lu, X.L., Liu, H.W. Electromagnetic Wave Absorbing and Mechanical Properties of Cement-based Composite Panel with Different Nanomaterials *Advanced Composites Letters* 26 (1) 2017: pp. 6–11. <https://doi.org/10.1177/096369351702600102>



© Sun et al. 2021 Open Access This article is distributed under the terms of the Creative Commons Attribution 4.0 International License (<http://creativecommons.org/licenses/by/4.0/>), which permits unrestricted use, distribution, and reproduction in any medium, provided you give appropriate credit to the original author(s) and the source, provide a link to the Creative Commons license, and indicate if changes were made.